applied nano

MDPI

Article

Effect of Heat Treatment on Polymorphism and Particle Size Distribution of Calcium Carbonate Nanoparticle Synthesized via Mechanochemical Process

Md Nuruzzaman [1,2], Yanju Liu [1,2], Mohammad Mahmudur Rahman [1,2], Saifullah Omar Nasif [1,2] and Ravi Naidu [1,2,*]

[1] Global Centre for Environmental Remediation (GCER), The University of Newcastle, University Drive, Callaghan, NSW 2308, Australia; md.nuruzzaman@newcastle.edu.au (M.N.); yanju.liu@newcastle.edu.au (Y.L.); mahmud.rahman@newcastle.edu.au (M.M.R.); saifullah.nasif@uon.edu.au (S.O.N.)

[2] crc for Contamination Assessment and Remediation of the Environment (crcCARE), University Drive, Callaghan, NSW 2308, Australia

* Correspondence: ravi.naidu@newcastle.edu.au or ravi.naidu@crccare.com

Abstract: The synthesis of calcium carbonate ($CaCO_3$) nanoparticles has gained an increasing interest due to their improved properties and diverse industrial applications. Among various synthesis techniques, the mechanochemical synthesis process has emerged as a promising route for nano-$CaCO_3$ synthesis. A high-energy ball mill is required for synthesizing nano-$CaCO_3$, whereas post-milling heat treatment facilitates completing the reaction that remains incomplete during milling. Post-milling heat treatment may also influence the properties of synthesized $CaCO_3$, which has not yet been thoroughly investigated. This study investigated the influence of post-milling heat treatment on the polymorphs, micromorphology, and particle size distribution of $CaCO_3$. The results indicated that the heat treatment of the as-milled powder enhanced the homogeneity of crystal polymorphs while maintaining the particle sizes within the nano-range (<100 nm). X-ray diffraction (XRD) analysis identified two polymorphs (vaterite and calcite) in samples obtained from different milling intensities. However, after heat treatment, all vaterite transformed into calcite. A bimodal particle size distribution was observed in $CaCO_3$ nanoparticles and was influenced by both the milling and heating intensities. It was observed that 60 min heat applied to 30 min as-milled powder was enough to produce nano-$CaCO_3$ (<50 nm) where the percentage of larger particles (<250 nm) became negligible (~1%). Micromorphology images confirmed the transformation of crystal polymorphs and the reduction in particle size.

Keywords: calcium carbonate; nanoparticle; mechanochemical process; heat treatment; calcite; vaterite; ball mill

Academic Editor: Angelo Maria Taglietti

Received: 4 February 2025
Revised: 30 April 2025
Accepted: 1 May 2025
Published: 6 May 2025

Citation: Nuruzzaman, M.; Liu, Y.; Rahman, M.M.; Nasif, S.O.; Naidu, R. Effect of Heat Treatment on Polymorphism and Particle Size Distribution of Calcium Carbonate Nanoparticle Synthesized via Mechanochemical Process. *Appl. Nano* **2025**, *6*, 8. https://doi.org/10.3390/applnano6020008

1. Introduction

Calcium carbonate ($CaCO_3$) is one of the most abundant and cost-effective inorganic minerals widely used across various industries including plastic, paper, rubber, paint, and ink [1–5]. In recent years, the application of ultrafine nano-$CaCO_3$ has increased due to its unique properties [6]. As a nano-sized particle, $CaCO_3$ serves as an effective filler or nucleating agent that enhances the penetration of $CaCO_3$ into polymeric matrixes [7]. Additionally, $CaCO_3$ nanoparticles improve the brightness and smoothness of products while enhancing their optical properties [7]. Beyond these applications, nano-$CaCO_3$ has been utilized in advanced applications such as serving as a template for synthesizing other

nanoparticles (e.g., hollow porous silica nanoparticles) [8] or as nano-carrier material in controlled delivery systems [9,10].

The increasing demand for nano-$CaCO_3$ in many fields has intensified research for its synthesis and characterization. However, its applicability largely depends on the specific polymorphic forms of $CaCO_3$ and their properties. Generally, $CaCO_3$ exists in multiple polymorphs, including amorphous calcium carbonate (ACC) and anhydrous crystalline phases such as calcite, aragonite, and vaterite. Additionally, it has also two hydrated phases, i.e., monohydrate and hexahydrate [7]. Among these, calcite is the most thermodynamically stable form, followed by aragonite and vaterite, while ACC is the least stable. The synthesis process plays a crucial role in determining the polymorphic forms of $CaCO_3$. So far, various synthesis processes such as wet chemical precipitation [8,9], reversed micelle [10,11], microemulsion [12,13], reverse microemulsion [14], and flame synthesis [15] have been employed for synthesizing nano-$CaCO_3$. In addition, the mechanochemical synthesis process has gained significant attention over the past decade. In this process, nano-$CaCO_3$ is synthesized using a high energy ball mill where the particle formation occurs due to solid-state displacement reactions among the precursors leading to nanoparticle formation [16–18]. This reaction is often referred to as a mechanically induced self-propagating reaction. This reaction is facilitated when highly exothermic powder mixtures are used [19]. Thus, the mixtures of $CaCl_2$ and Na_2CO_3 or K_2CO_3 are mostly used for the mechanochemical synthesis of nano-$CaCO_3$.

In mechanochemical synthesis, collisions and friction between the balls, as well as between the balls and the walls of the milling chamber, are responsible for the deformation, fragmentation, mixing, and cold-welding of the starting materials [20,21]. Thus, the mechanical activation of reactants or precursors reaches a critical point known as the ignition time, where the reaction rates begin to accelerate. This increase in reaction rates raises the temperature within the milling system, leading to a reaction that resembles thermally ignited self-propagating high-temperature synthesis [18]. However, the ignition time can vary from a few seconds to several hours, depending on the specific reaction and milling conditions. For instance, synthesizing nano-$CaCO_3$ in a SPEX8000 ball mill required 4 h of milling, whereas using a planetary or attrition type of ball mill reduced the milling time to just 10 min [16,17]. It was observed that the ball temperature in the SPEX 8000 shaker mill remained below 100 °C. However, under similar intensities, the ball temperature in a planetary ball mill was found to exceed 200 °C [22]. Therefore, synthesizing nano-$CaCO_3$ required less time in a planetary ball mill compared to the SPEX 8000 ball mill. Tsuzuki and co-workers also observed that the reaction between the starting materials in the SPEX 8000 ball mill was incomplete [16]. As a result, post-milling heat treatment was applied to complete the reaction.

The formation of nanostructured materials is also governed by a diffusion process among the precursors or reactants, influenced by thermal activity in the milling chamber. Several milling parameters affect the temperature generated during milling. In this context, the one-step mechanochemical synthesis of nano-$CaCO_3$ is feasible if the milling process generates sufficient heat in the milling chamber [17]. Along with the type of ball mill, various milling parameters such as the materials of the milling media, the ball-to-powder ratio, the extent of filling in the milling chamber, the milling atmosphere (temperature and pressure), and the milling time significantly impact particle size distribution [23,24]. Therefore, the optimization of these milling parameters is essential to achieve particle sizes within the nano-range [25]. Moreover, the desired particle size distribution of nano-$CaCO_3$ can also be achieved by adjusting the amount of diluent such as halite (NaCl) used during milling. For instance, Tsuzuki et al. found that increasing the molar ratio of diluent (NaCl) to reactants from 3.5 to 10.3 led to a significant reduction in particle size [16]. However,

excessive diluent in the milling chamber is not suitable for the commercial production of $CaCO_3$ nanoparticles as it reduces production efficiency and increases cost.

It is necessary to reduce the limitations of nano-$CaCO_3$ synthesis using mechanochemical process, such as prolonged milling time and dependency on specific types of ball mills, and to minimize the use of large amounts of salt matrix during the synthesis of $CaCO_3$ nanoparticles. To overcome such limitations, heating the as-milled powder can be an effective tool for synthesizing $CaCO_3$ nanoparticles [16]. Even though Tsuzuki et al. (2000) [16] suggested that heating the as-milled powder could increase the crystallinity of nanoparticles but was not investigated thoroughly. Consequently, heat treatment can also influence the polymorphs and particle size distribution [26,27]. Therefore, this study investigated the effect of heat treatment on the crystallinity, micromorphology, and particle size distribution of $CaCO_3$ nanoparticles that were synthesized using only 1 mole NaCl as diluent and at three different milling intensities. It is expected that the combination of both milling and heating time will simplify the synthesis process, making nano-$CaCO_3$ production more efficient and scalable.

2. Materials and Methods

2.1. Chemicals and Reagent

The chemical required anhydrous $CaCl_2$ granules ($\geq$93.0%, $\leq$7 mm beads), Na_2CO_3 (99.5%), and NaCl ($\geq$99.5%) were purchased from Merck, Truganina, VIC, Australia. All the chemicals were dried in an oven at 105 °C for 12 h prior to use.

2.2. Synthesis of $CaCO_3$ Nanoparticles

In this experiment, $CaCO_3$ was synthesized by a solid-state displacement reaction following the procedure described earlier [16,17] but with a lower amount of diluent, i.e., halite (Equation (1)).

$$CaCl_2 + Na_2CO_3 + NaCl \rightarrow CaCO_3 + 3NaCl \quad (1)$$

The stoichiometric mixture of the starting materials and the diluent (NaCl) was milled together using a planetary ball mill (Nuoya NQM series 0.4 L, Jiangsu, China). The milling jar was made from stainless steel; it had a depth and radius of 40 mm and 45 mm, respectively, and the cubage of the jar was 50 mL. Two different sizes of steel balls were used during milling, with radii of 10 mm and 6 mm. The respective ball weights were 4.108 ($\pm$0.008) g and 0.885 ($\pm$0.003) g. The ball-to-powder ratio was 20:1 where filling the jar did not extend beyond 50%, and milling speed was 350 ($\pm$5) rpm. The milling process lasted from 10 min to one hour, and the as-milled powder was heated at 390 °C for 0, 30, 60, and 120 min using a muffle furnace. A portion of the synthesized powder was washed with Milli-Q water (ELGA Labpure System, resistivity 18.2 Ω) several times to remove NaCl. In the washing process, the powder was put in a glass beaker, then Milli-Q water was added and stirred for 2 h using a magnetic stirrer. The supernatant was discarded via centrifugation. This process continued until the NaCl was completely removed. Finally, the washed powder was dried in an oven at 60 °C. Both the washed and unwashed (as-milled) powder was kept in a desiccator prior to further characterization while the washed powder was dried in an oven at 60 °C for 24 h prior to preservation. The overall synthesis procedures of nano-$CaCO_3$ are presented in Figure 1.

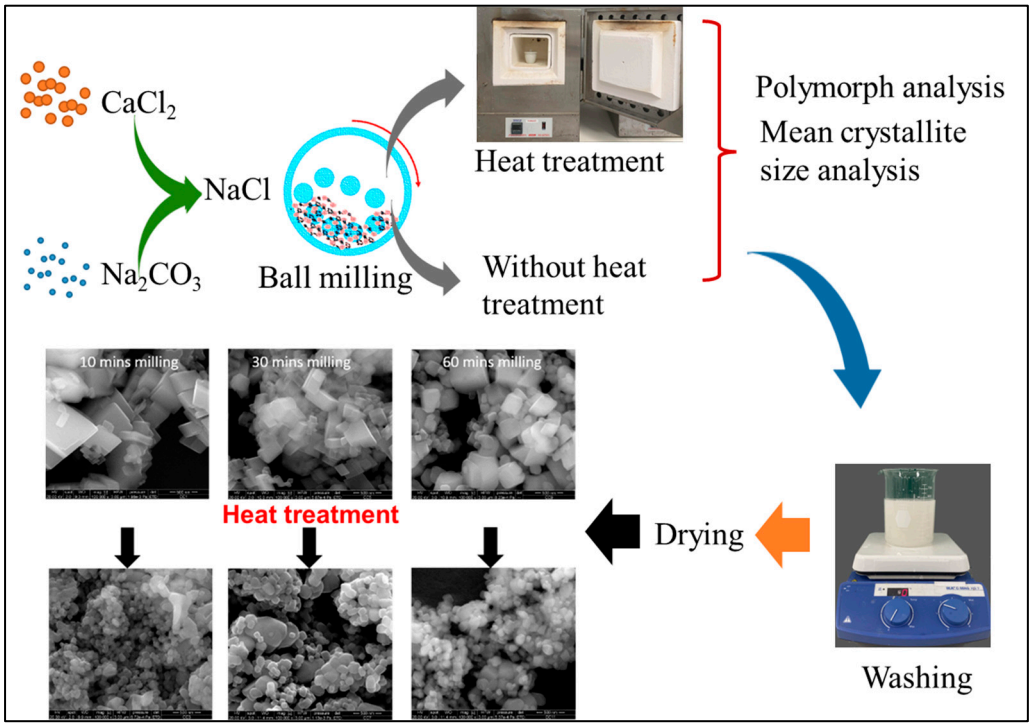

Figure 1. Synthesis of $CaCO_3$ nanoparticles via mechanochemical process.

2.3. Characterization of the Milled Powder and $CaCO_3$ Nanoparticles

Of the different characterizations, the X-ray diffraction (XRD), thermogravimetric analysis (TGA), and differential scanning calorimetry (DSC) of the as-milled powder were carried out using the unwashed powder (i.e., containing NaCl), whereas particle size analysis was carried out using the washed powder (i.e., after removing NaCl), and micromorphology analysis was performed using both washed and unwashed powder samples.

2.3.1. X-Ray Diffraction Analysis and Crystallite Size Measurement

The phase composition of as-milled powder samples was analyzed using X-ray diffraction (XRD). For analysis, the same amount of powder samples was loaded into a stainless-steel sample holder using the back-loading method [28]. XRD patterns were obtained using Cu-Kα radiation (λ = 1.5418 Å) on a PANalytical, Empyrean X-ray diffractometer (PANalytical Specters Australia Pty. Ltd., Welshpool, Australia) operating at 40 kV and 40 mA. The patterns were collected from 10° to 70° (2θ degrees) with a step size of 0.013° (2θ degrees) on continuous scanning. The phase identification of $CaCO_3$ present in the as-milled powder (both with and without heat treatment) was performed by comparing sample patterns with the ICDD database upgraded in the PANalytical X'Pert Highscore Plus software (version 4.7). The file references were also used to compare calcite with the standard calcite. The mean crystallite size was calculated from the diffraction peak following the Cauchy–Gaussian equation (Figure S4).

2.3.2. Thermogravimetric Analysis and Differential Scanning Calorimetry

TGA and DSC measurements were conducted to investigate the thermal behavior of the milling powder using the Mettler Toledo TGA/DSC 1 device. The powder sample (around 20 mg) was heated up to 900 °C using a 70 µL platinum crucible. The heating rate was 10 °C min^{-1} under a constant N_2 gas flow at 50 mL min^{-1}.

2.3.3. Micromorphology Analysis

The micromorphology of the synthesized nano-$CaCO_3$ was examined by a FEI Quanta 450 FEG environmental scanning electron microscope (ESEM) using an accelerating voltage of 20 kV. The $CaCO_3$ powder samples were put on the carbon substrate's surface, followed by the application of 10 nm carbon coatings over the sample using a Quorum (Q 150T ES) Turbo-Pumped Sputter Coater for imaging.

2.3.4. Particle Size Analysis

The particle size distributions were analyzed using a Nicomp 380ZLS particle size analyzer (Particle Sizing Systems, Santa Barbara, CA, USA) using the dynamic light scattering (DLS) technique. The mean particle sizes and their distribution were obtained using number-weight Nicomp distribution analysis. Each of the dried $CaCO_3$ samples was suspended in Milli-Q water (0.05% w/v) and stirred for 2 h, followed by sonication for 15 min before particle size analysis.

2.3.5. Surface Area Analysis

The specific surface area was measured by Brunauer–Emmett–Teller (BET) and the Langmuir N_2 gas adsorption method using a Micrometrics Gemini-V surface area and pore size analyzer at −197 °C. Both the reference and the sample tube were dipped into the liquid N_2 to maintain the homogeneous environment during analysis.

3. Results and Discussion

3.1. Polymorphs of $CaCO_3$ Nanoparticles

In XRD patterns of the as-milled powder, diffraction peaks of $CaCO_3$ were identified after 10 min milling, indicating that the chemical reaction between $CaCl_2$ and Na_2CO_3 took place within 10 min continuous milling (Figures 2 and S1). No corresponding peaks of $CaCl_2$ and Na_2CO_3 were identified in the XRD spectrum of 10 min as-milled powder, indicating the completion of the reaction among the precursors (Figure S1). A similar result was obtained in a previous study where $CaCO_3$ was detected after 10 min milling of $CaCl_2$ and Na_2CO_3 [17]. This finding suggests that 10 min milling is sufficient for the mechanochemical activation of $CaCl_2$ and Na_2CO_3 when they are milled together using a high-energy planetary ball mill.

In the XRD patterns of the as-milled powder, two crystalline polymorphs of $CaCO_3$—vaterite and calcite—were identified (Figure 2a,b). The diffraction peaks of vaterite were identified with 2θ values around 24.87°, 32.71°, 43.80°, and 50.1°, which can be assigned to crystal planes (110), (114), (300), and (104) (ICDD PDF: 72-0506). The diffraction peaks of calcite were identified with 2θ values around 23.06°, 29.41°, 35.98°, 39.42°, 43.17°, 47.13°, and 47.53°, and correspond to the crystal planes (012), (104), (110), (113), (202), (018), and (116) (ICDD PDF: 83-0577). The diffraction peaks of halite were identified with 2θ values of approximately 27.45°, 31.79°, 45.53°, 53.94°, and 56.57°, corresponding to the (111), (200), (220), (311), and (222) planes (ICDD PDF: 05-0628). In the diffraction pattern of the as-milled powder, the major peak corresponded to halite (200) as it was used as a diluent during milling and produced as a by-product. It was observed that milling time played a significant role in the formation of the two crystalline polymorphs of $CaCO_3$. The XRD patterns of the as-milled powder showed that all the calcite peaks became more intense with increasing milling time from 10 min to 60 min, whereas the opposite trend was observed for vaterite peaks (Figure 2b). Because vaterite is the least stable polymorph of $CaCO_3$, it was gradually converted into the most stable calcite by the action of heat that was generated from the continuous ignition of the materials in the milling chamber. Thus, the formation of calcite was facilitated with increasing milling time. In a previous study, a

similar gradual transformation of vaterite into calcite was also reported when chemically synthesized vaterite (93.6%) and calcite (6.4%) were milled together [29].

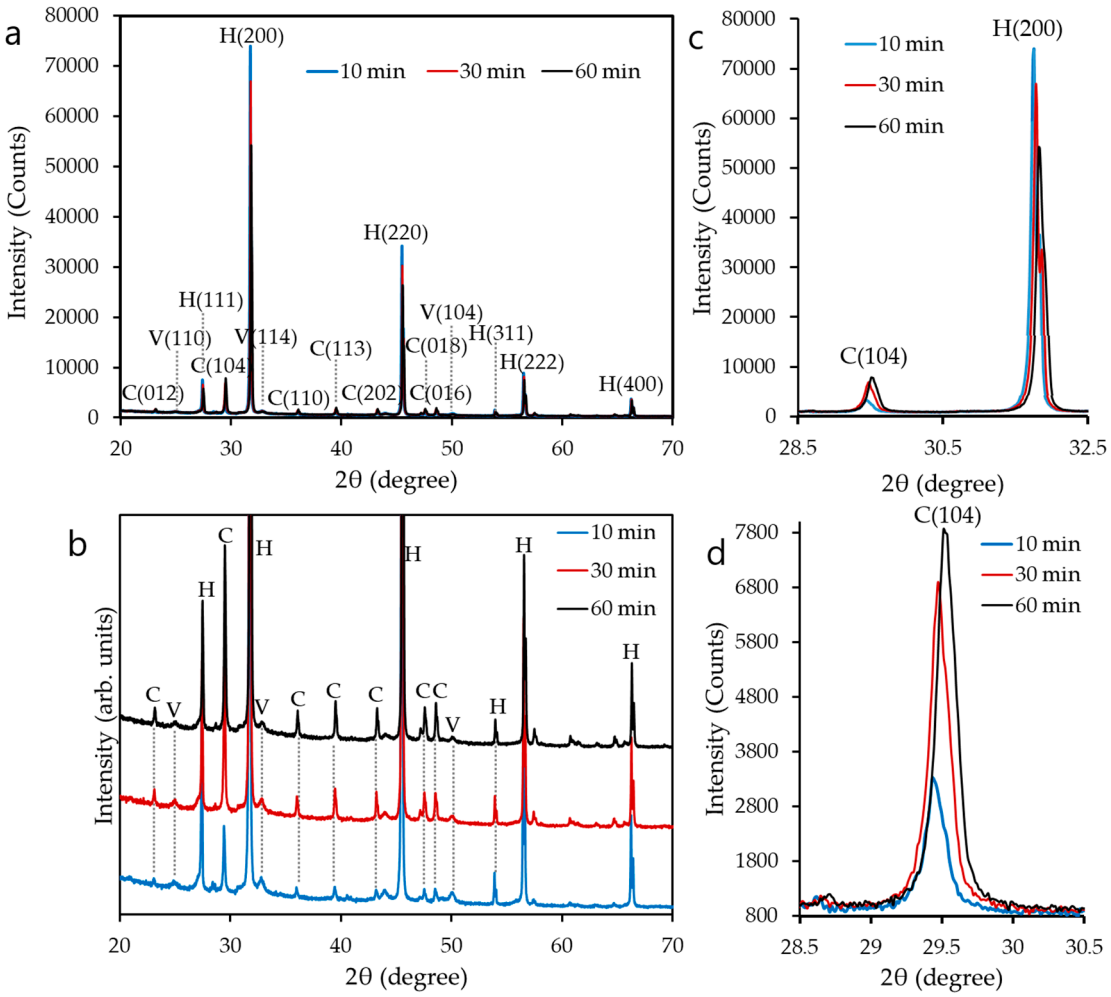

Figure 2. XRD patterns of as-milled powder (**a**,**b**); major peaks of calcite and halite (**c**); and major peaks of calcite (**d**) obtained from different milling durations. H—halite; C—calcite; V—vaterite.

This transformation can also be represented by the peak intensities of calcite and halite (Figure 2a). For instance, the peak intensity of calcite (104) increased with increasing milling time from 10 min to 60 min while the peak intensity of NaCl (200) decreased (Figure 2c). Likewise, the intensities of other calcite peaks also increased while the NaCl peaks decreased with increasing milling time. Furthermore, shifting in the peak position of calcite and halite was observed with increasing milling time. Though the shifting in peak position was not that much, all the peaks shifted from a lower 2θ to a higher 2θ angle with increasing milling time from 10 min to 60 min. Shifting in peak position also represents changes in the d-spacing value where the d-spacing value decreases with an increase in the corresponding 2θ position of the peak, and vice versa (Tables S1 and S2). Figure 2d represents the shift in peak position of calcite (104). A decreasing trend in d-spacing values was also observed in calcite peak (104) with an increase in the corresponding 2θ position of the peak with increasing milling time (Table S1). Changes in the 2θ position have effects on Bragg's angle and ultimately change the crystallite size. In general, the crystallite size decreases with an increase in corresponding 2θ position of the peak, and vice versa. The increase in peak height further confirmed the formation of new crystals of calcite (Figure 2d). However, 60 min of milling was insufficient to convert of all the vaterite

into calcite, as the vaterite peaks, although much weaker, were still observed in the XRD spectrum (Figure 2b).

Similarly, the heat treatment of the as-milled powder also contributed significantly to the transformation of the crystalline polymorphs of $CaCO_3$ (Figures 3, S2 and S3). When heat was applied to the as-milled powder, all the vaterite peaks disappeared and influenced the calcite peak intensity (Figures 3b, S2b and S3b). It was observed that after 30 min heating, the peak intensity of calcite (104) in 10 min as-milled powder was not as much as it was observed when heat was applied for 60 min to 120 min (Figure 3d and Table S1). This indicates the presence of either an amorphous or transition phase of $CaCO_3$ in the 10 min milling powder, whereas 30 min heat was not enough to convert the other phases into calcite. No significant difference in the peak height of calcite (104) was found to the 10 min milled powder when heat was applied for 60 min to 120 min (Figure 3d). This result indicated that post-milling heat treatment for 60 min was sufficient to obtain complete conversion of other phases to calcite.

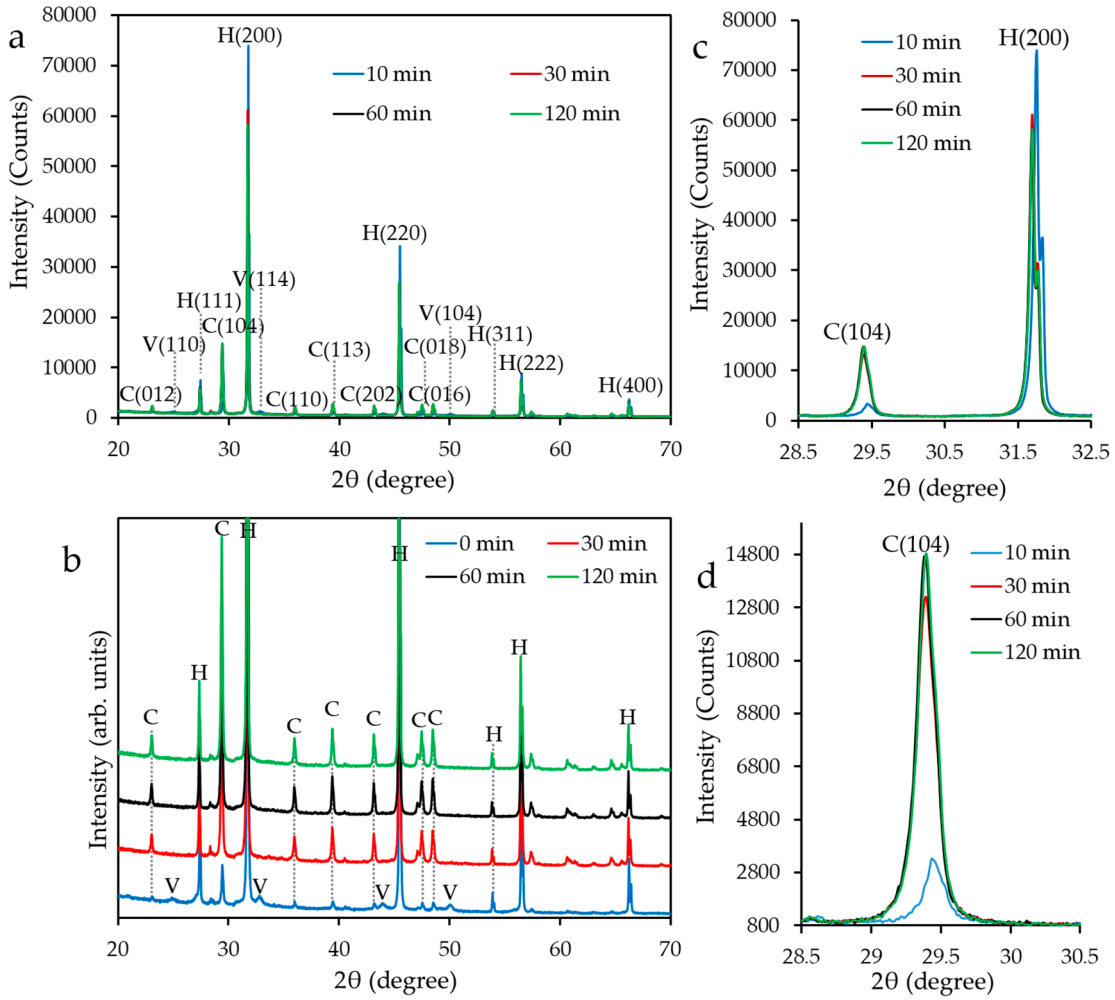

Figure 3. XRD patterns of 10 min as-milled powder (**a**,**b**); major peaks of calcite and halite (**c**); and major peaks of calcite (**d**) obtained after heat treatment. H—halite; C—calcite; V—vaterite.

A similar result was observed when the heat was applied to 30 min and 60 min as-milled powder (Figures S2 and S3). Additionally, the calcite (104) peak intensity reached its maximum after 60 min heating but slightly decreased when the heating time was increased to 120 min (Table S1). This reduction could be attributed to the recrystallization of ultrafine $CaCO_3$ facilitated via prolonged heat treatment. The recrystallization process was evident

from the shifting in the peak position of calcite (104) from a higher 2θ angle to a lower 2θ angle indicating changes in d-spacing values (Figure 3d, Figures S2d and S3d). In addition, peak broadening values could be represented by the full width at half maximum (FWHM) of the peak (Equation (S1)). It was observed that the FWHM values of calcite (104) increased with heat treatment (Table S1), indicating the reduction in crystallite size. Further, all the halite peaks (200) were dendritic in nature, which indicated broad or diffuse peaks. Shifting in the peak position was also observed after heat treatment (Table S2). Thus, these variations can also indicate the changes in the crystallinity or crystal size of halite.

3.2. Mean Crystallite Size

The mean crystallite sizes of $CaCO_3$ obtained from different treatments are presented in Table 1. It was observed that heat treatment did not affect the average crystallite size present in the as-milled powder. However, the smallest crystal size formed when the precursor materials were milled for 60 min, followed by heat treatment for 120 min.

Table 1. Mean crystallite sizes of $CaCO_3$ (calcite) obtained through XRD peaks under various experimental conditions.

Milling Time (min)	Heating Time			
	0 min (nm ± SD)	30 min (nm ± SD)	60 min (nm ± SD)	120 min (nm ± SD)
10	56.9 ± 10.16	58.3 ± 4.95	56.4 ± 3.59	57.5 ± 4.03
30	51.2 ± 3.49	52.4 ± 3.42	56.1 ± 3.43	55.0 ± 2.59
60	51.3 ± 3.64	48.2 ± 2.88	49.1 ± 3.63	41.3 ± 2.05

3.3. TGA and DSC Analysis

TGA/DSC measurements were carried out to understand the thermodynamic transformation characteristics of the products present in the as-milled powder without any heat treatment (Figure 4). The XRD analysis confirmed the presence of calcite, vaterite, and halite in the milled powder. The TGA and DTG (Derivative Thermogravimetry) curves showed weight loss below 260 °C (Figure 4a,b). This mass loss was mainly due to the removal of absorbed water [30]. It was observed that by increasing milling time from 10 min to 60 min, the amount of absorbed water decreased from 11.08 to 8.05%. A further weight loss occurred between 540 and 780 °C, which was attributed to the release of CO_2 during the decomposition of $CaCO_3$ into CaO. At this stage, all as-milled powder exhibited a weight loss of around 12.45%, indicating the presence of the same amount of $CaCO_3$. In addition, less than 0.5% weight loss occurred between 460 and 540 °C in all as-milled powder. This weight loss corresponded to the removal of entrapped crystalline water or adsorbed water [31].

No significant weight loss was observed between 260 and 460 °C; however, an exothermic peak was detected in the DSC curves at 282 °C (Figure 4c), indicating that a phase transformation of $CaCO_3$ occurred around this temperature. This observation was further supported by the first derivative of heat flow curves of the as-milled powders (Figure 4d). In a previous study, a sharp exothermic peak was observed at 327 °C during the DSC analysis of the ACC corresponding to the conversion of ACC to calcite [32]; however, no calcite peaks were detected in the XRD spectrum when ACC was heated at 330 °C. Calcite peaks were only observed in the XRD pattern when the ACC powder was heated to 360 °C with further intensification at 390 °C [32]. In another experiment, a sharp exothermic peak was also observed at 326 °C for the crystal transformation of ACC [30]. In their study, Tsuzuki et al. obtained an exothermic peak at 295 °C in the DTA curve and claimed that the peak indicates the reaction temperature between the starting materials [16]. However,

they obtained the exothermic peak in 4 h milling powder where no peak of the starting materials was observed. Thus, the exothermic peak in the DSC or DTA curve observed around 290–330 °C may indicate the presence of a metastable phase or an amorphous phase in the milling powder that starts to convert into calcite around that temperature.

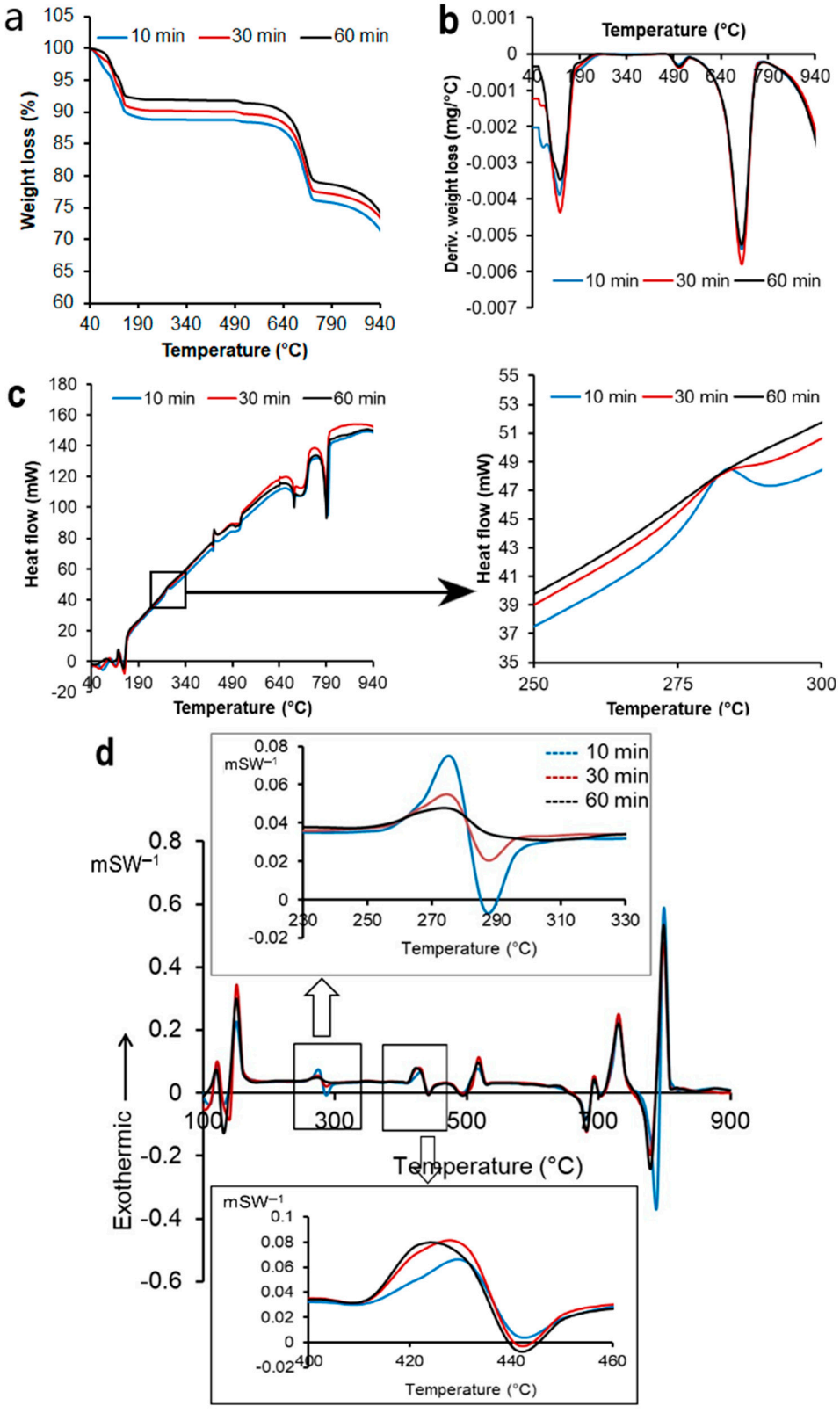

Figure 4. Showing TGA curves (**a**), DTG curves (**b**), heat flow curves (**c**) and first derivative of heat flow curves (**d**) of as-milled powder (without heat treatment).

In this study, the milling powder was heated at 390 °C to ensure the transformation of metastable phases to stable calcite (e.g., vaterite to calcite). The crystallization peak appearing at 282 °C was most pronounced in the milling powder that was milled for 10 min, confirming the existence of a more metastable phase of $CaCO_3$ in the milling powder (Figure 4d). The DSC peaks of the as-milled powder at 282 °C indicated the possible presence of ACC in the as-milled powder [30,32]. However, the XRD patterns of the as-milled powder failed to explain the presence of ACC in the milling powder (Figure 2). This may be due to the presence of a very low amount of ACC content comparative to other components (e.g., NaCl, calcite, and vaterite). Further, another exothermic peak was observed at 432 °C in the DSC curve (Figure 4d) where there was no weight loss in TGA (Figure 4a). The exothermic peak could be reasonably explained by the fact that high-energy-state vaterite transformed to a lower-energy-stable state of crystalline calcium carbonate and released the energy of the system. These findings demonstrated that heat treatment, combined with increasing milling time, significantly influences the polymorphic transformation of $CaCO_3$.

3.4. Effect of Milling and Heating Time on Particle Size Distribution

To measure the mean particle size of synthesized $CaCO_3$ obtained from different milling and heating times, all the powder samples were washed properly to remove all the NaCl. It was observed that both milling time and the heat treatment of the as-milled powder significantly influenced particle size distribution (Table 2). In all the samples, a bimodal particle size distribution (grouped as peak 1 and peak 2) of synthesized $CaCO_3$ was observed (Figure 5 and Figure S6). The particle size distribution of $CaCO_3$ obtained from only milled powder showed that the mean particle size was reduced with increasing milling time from 10 min to 60 min (Table 2). In peak 1, the particle size was reduced from 189.0 (±30.2) nm to 113.0 (±10.3) nm with increasing milling time from 10 min to 30 min, but further milling up to 60 min increased the particle size to 151.6 (±23.2). However, in peak 2, the particle size was reduced from 605.5 (±104.6) nm to 432.5 (±70.2) nm with increasing milling time from 10 min to 60 min (Table 2).

Table 2. Mean particle size distribution of synthesized $CaCO_3$ under various experimental conditions.

Milling Time (min)	Peak 1			Peak 2		
	Size (nm)	SD (nm)	%	Size (nm)	SD (nm)	%
0 min heat						
10	189.0	30.2	78.3	605.5	104.6	21.7
30	113.0	10.3	88.3	477.1	81.2	11.7
60	151.6	23.2	85.1	432.5	70.2	14.9
30 min heat						
10	88.4	14.9	94	247.0	39.7	5.9
30	64.3	8.6	98	247.5	36.7	1.9
60	66.6	9.6	99	277.8	38.8	0.9
60 min heat						
10	65.2	12.2	97.1	259.9	35.3	2.9
30	47.1	7.4	99.3	235.4	27.9	0.7
60	48.1	6.1	99.4	218.1	25.2	0.6
120 min heat						
10	68.2	12.9	98.6	277.8	45.1	1.4
30	52.6	7.9	99.6	249.3	43.5	0.4
60	52.5	7.1	99.9	228.0	12.3	0.1

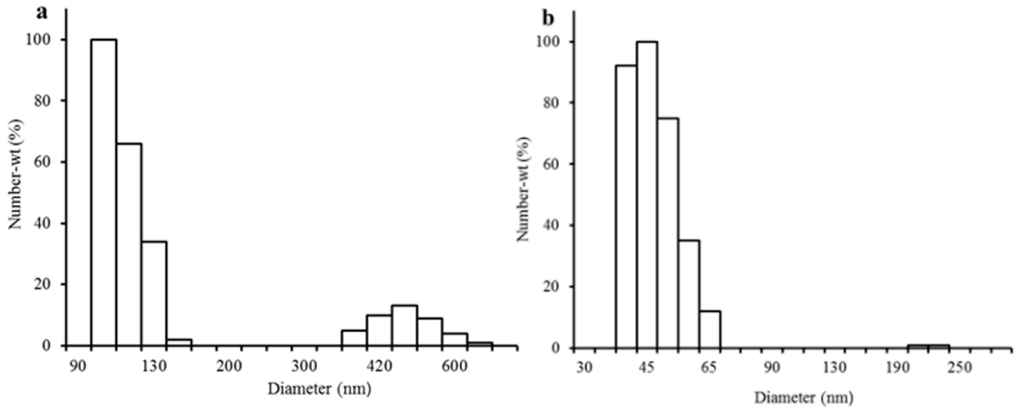

Figure 5. Particle size distributions of 30 min milled powder heated for 0 min (**a**) and 60 min (**b**).

However, heat treatment reduced the particle size distribution in a way that the percentage of bigger particles became negligible (~1%). Therefore, after milling, heat treatment was found to be an effective tool for reducing the particle size within the nano-range with a low amount of diluent (1 mole NaCl) (Equation (1)). In peak 1, the smallest mean particle size was found when 30 min milled powder was heated for 60 min whereas in peak 2, the smallest mean particle size was found when 60 min milled powder was heated for 60 min (Table 2 and Figure S6). No significant difference in mean particle size was found when the powders milled for 30 min and 60 min were subsequently heated for 60 min and 120 min. From Table 2, it is observed that heat treatment up to 60 min reduced the mean particle size but when the heating time increased, the particle size also started to increase. It is notable that although particle size began increasing at 120 min heating time, the number of larger particles decreased.

In this study, a bimodal particle size distribution was observed due to the utilization of a low amount of diluent (1 mole NaCl). However, the amount of $CaCO_3$ synthesis was increased in the milling powder. In an earlier study, the particle size was distributed from 60 nm to 240 nm when 3.5 mole NaCl was used, and the particle size distribution was 20 nm to 130 nm when the amount of NaCl increased to 10.3 mole in the milling chamber [16]. The results of this study also showed that heat in the milling chamber or applied externally after milling has the capacity to influence the crystallization process which affects the particle size. Also, particle size exhibited a tendency for unimodal distribution, but the mean particle size became larger. Therefore, an increased height was observed at the major peak of calcite (104) in the XRD pattern when the 30-to-60 min as-milled powder was heated for 60 min compared to 120 min. The increase in the particle size with an increase in the heating time can be explained by the Ostwald ripening effect where the small particles are dissolved into large particles during the transformation of a metastable phase to a stable calcite phase due to heat treatment or washing time [33]. Thus, external heat proved to be more effective when it was applied after a certain milling time in which the particle size was found to be minimal or finest.

Further, to clarify the effect of diluent concentration, the $CaCO_3$ was synthesized with a highly concentrated diluent ($CaCl_2 + Na_2CO_3 + 7NaCl \rightarrow CaCO_3 + 9NaCl$). The starting materials were milled for 10, 30, and 60 min, followed by heat treatment at 390 °C for 0, 60, and 120 min using a muffle furnace. The 10 min as-milled powder samples (without washing) were analyzed using XRD as mentioned earlier (Section 2.3.1). In the XRD pattern, the vaterite was the main polymorph of $CaCO_3$ in the 10 min as-milled powder (Figure 6a). All the vaterite $CaCO_3$ was converted to calcite when the 10 min as-milled powder samples were heated for 60 min to 120 min. In addition, a unimodal particle size distribution of

$CaCO_3$ was observed when the 60 min as-milled powder was heated for 120 min. The average particle size was distributed from 30 nm to 50 nm (Figure 6b).

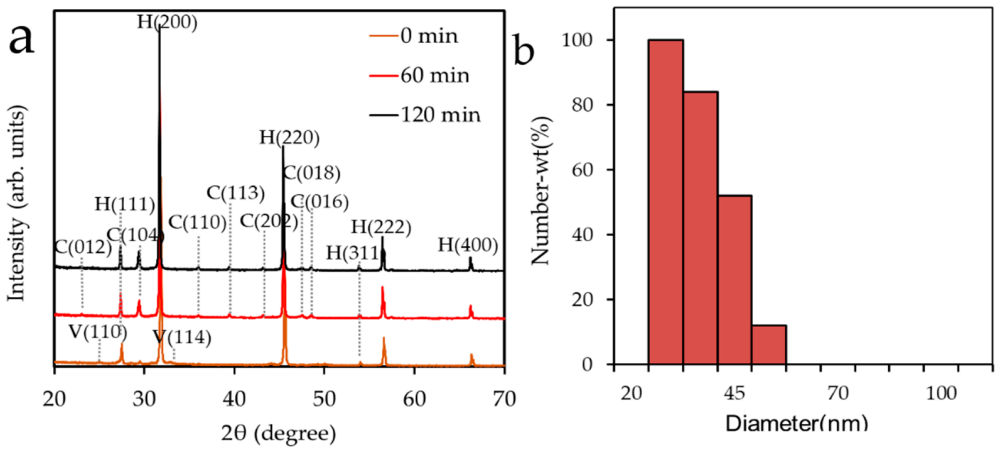

Figure 6. XRD patterns of 10 min as-milled powder (as per $CaCl_2 + Na_2CO_3 + 7\ NaCl \rightarrow CaCO_3 + 9\ NaCl$) heated for 0 min, 60 min, and 120 min (**a**), and particle size distributions of 60 min milled powder heated for 120 min (**b**). H—halite; C—calcite; V—vaterite.

3.5. Micromorphology Analysis of Synthesized $CaCO_3$

The micromorphology analysis of the as-milled powder confirmed the formation of two different $CaCO_3$ polymorphs, i.e., vaterite and calcite, present in the 10 min as-milled powder (Figure 7). This result indicated that 10 min milling was sufficient for the formation of $CaCO_3$. This observation supports the results obtained by the XRD analysis where both vaterite and calcite peaks were detected in the XRD patterns of the as-milled powder (without any heat treatment). The EDX spectra also confirmed the presence of halite (NaCl) in the as-milled powder (Figure 7).

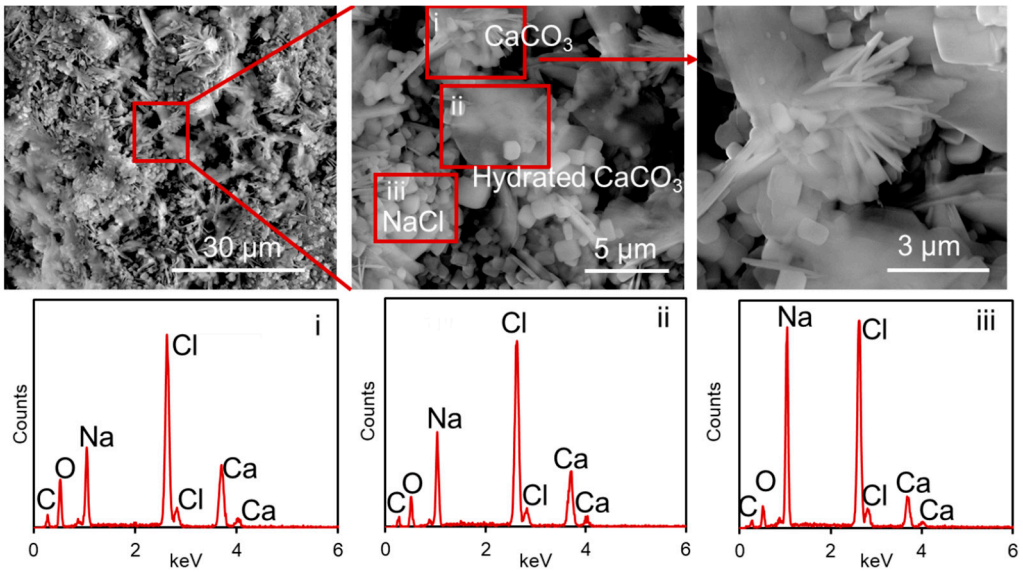

Figure 7. The ESEM images and EDX spectra of milling powder milled for 10 min show the formation of two polymorphs of $CaCO_3$ in the presence of NaCl.

Similar morphological features were also observed in the 60 min as-milled powder; however, the morphology of the 30 min as-milled powder showed different morphological features. An aggregation of the components was observed in the 30 min as-milled powder (Figures 8 and S6). However, only the calcite phase was observed in the milling powder

when NaCl was removed by washing with water (Figures 8, S7 and S8). This was due to the conversion of unstable vaterite into calcite. An earlier study showed that the transformation of unstable $CaCO_3$ such as ACC to calcite occurred either in the presence of water or when heat was applied [32]. Therefore, it is necessary to investigate the as-milled powder before the removal of NaCl to assess the effect of the ball milling process on the polymorphism of $CaCO_3$.

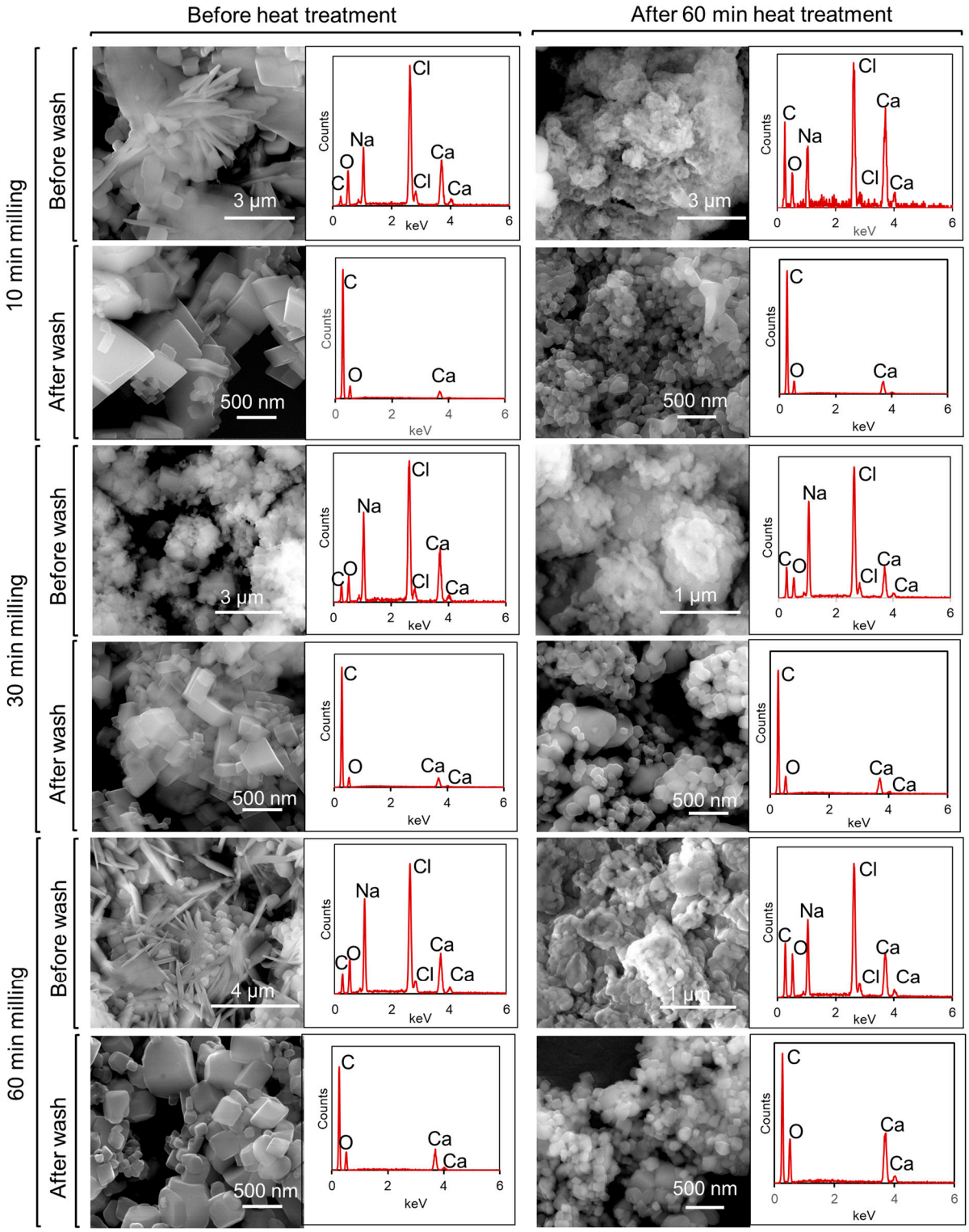

Figure 8. ESEM images of $CaCO_3$ nanoparticle obtained from 10 min, 30 min, and 60 min milling before (0 min) and after 60 min heat treatment.

The ESEM images also showed that the particle size is influenced by the milling time (Figure S7), whereas the micromorphology of the post-milling heated powder showed that the heat treatment of the as-milled powder played a crucial role in changing the polymorphs of $CaCO_3$ as well as the particle size distribution (Figures 8, S7 and S8). After the heat treatment of the milled powder, particle coarsening was observed, indicating the phase transformation of $CaCO_3$ to its stable calcite polymorph (Figure S6). The aggregates were formed of $CaCO_3$ particles blended with NaCl. The effect of external heat and milling time on the reduction in particle size was more clearly observed through the ESEM images of the washed samples (Figures 8, S7 and S8). The images present a similar trend in particle size to the one that was found in the results of the particle size analyzer. Heat treatment drastically reduced the particle size to less than 100 nm (Figure S7).

In addition, the role of diluent in changing the morphology of $CaCO_3$ was investigated using a higher amount of diluent (7 mole NaCl). It was observed that when 7 mole NaCl was used during milling, a dumbbell-shaped vaterite was formed in the 10 min as-milled powder (Figure S9). The vaterite phase remained stable after the removal of NaCl, forming spherical vaterite with a particle size less than 500 nm (Figures 9 and S10). However, when heat was applied to the 10 min as-milled powder, the morphology of $CaCO_3$ was significantly changed. With 60 min heat treatment, the vaterite polymorphs converted to calcite (Figure S9). However, only calcite was found after removing the diluent, with a particle size less than 100 nm (Figures 9b and S10). The particle size remained below 100 nm even with the 120 min heat treatment of the 10 min as-milled powder (Figures 9c and S10c). With increasing milling time up to 60 min, a well-dispersed powder mixture was observed where calcite was formed after the removal of NaCl. The heat treatment of the 30 min and 60 min as-milled powder for 60 min significantly reduced the particle size (Figure S9).

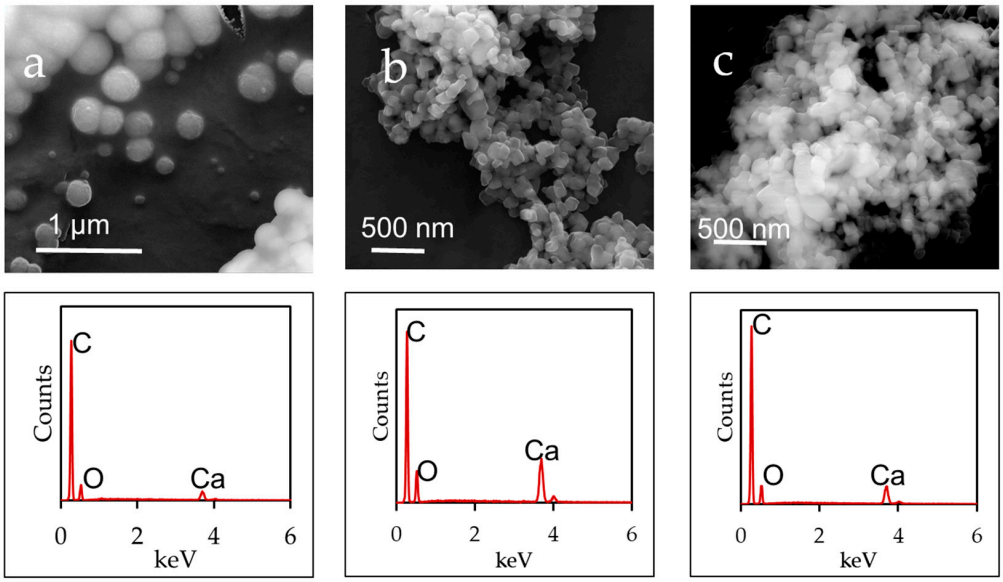

Figure 9. ESEM images of $CaCO_3$ obtained from 10 min milled powder and heated for 0 min (**a**), 60 min (**b**), and 120 min (**c**) after removal of NaCl as per $CaCl_2 + Na_2CO_3 + 7\ NaCl \rightarrow CaCO_3 + 9\ NaCl$.

3.6. Surface Area

It is reasonable that the nanoparticles' performance depends on their surface behavior. Therefore, the surface area of synthesized $CaCO_3$ was analyzed (Table 3). Similar trends were observed in both the BET surface area and the Langmuir surface area. The surface area expanded with increased milling time and heating time. The maximum surface area was obtained from the sample milled for 60 min and heated for 120 min whereas the minimum surface area was found at 10 min milling without any heat treatment. It

is expected that the surface area could be increased further with an increasing amount of diluent. Increasing the amount of diluent can reduce the particle size [16] as well as inhibiting particle agglomeration during mechanochemical synthesis [34].

Table 3. Mean BET and Langmuir surface areas of $CaCO_3$ synthesized under various experimental conditions.

Milling Time (min)	Heating Time (min)			
	0	**30**	**60**	**120**
	Mean BET surface area (m^2g^{-1})			
10	3.8	6.9	6.2	6.6
30	3.9	7.8	7.5	7.4
60	6.0	7.8	7.6	8.6
	Langmuir surface area (m^2g^{-1})			
10	5.5	9.9	9.0	9.9
30	5.6	11.3	10.8	10.8
60	8.6	11.3	11.0	12.4

4. Conclusions

The synthesis of $CaCO_3$ using a ball mill is an easy route where particle size and polymorphs vary with milling time. The heat treatment of the as-milled powder effectively reduced the particle size and increased the homogeneity in crystal polymorphs. Without heat treatment, two different crystal polymorphs (vaterite and calcite) were formed that transformed into calcite after heat treatment. Approximately 36% of the nano-$CaCO_3$ was produced due to the utilization of 1 mole of NaCl as diluent. Due to the lower amount of diluent content in the milling chamber, a bimodal particle size distribution was observed. A combination of 30 min milling followed by 60 min heat treatment of the as-milled powder was enough for synthesizing nano-$CaCO_3$. The particle size was around 50 nm, and the number of larger particles (~250 nm) became negligible (<1%). Thus, a combined milling and heating process simplifies the synthesis of nano-$CaCO_3$. The simplified synthesis procedure used in this study shows promise for large-scale industrial applications due to the cost-effectiveness and accessibility of heat treatment in industrial practice, along with the straightforward operation of ball milling.

Supplementary Materials: The following supporting information can be downloaded at: https://www.mdpi.com/article/10.3390/applnano6020008/s1, XRD patterns of precursors and as-milled powder, Measurement of crystallite size, Particle size distribution, Morphology of synthesized $CaCO_3$, Morphology of synthesized $CaCO_3$ using 7 NaCl.

Author Contributions: M.N. conceived the project, performed the experiments, processed the data, and wrote the original draft. Review and editing were conducted by M.N., Y.L., M.M.R., S.O.N. and R.N. Visualization was carried out by M.N. and S.O.N. R.N. supervised the overall project. All authors have read and agreed to the published version of the manuscript.

Funding: This research received no external funding.

Data Availability Statement: This is to declare that the data of this work will be available on request from readers.

Acknowledgments: The first author is grateful to the crc for Contamination Assessment and Remediation of the Environment (crcCARE), The University of South Australia, and The University of Newcastle for research support.

Conflicts of Interest: The authors declare no conflicts of interest.

Abbreviations

The following abbreviations are used in this manuscript:

ACC	amorphous calcium carbonate
BET	Brunauer–Emmett–Teller
$CaCO_3$	calcium carbonate
DSC	differential scanning calorimetry
XRD	X-ray diffraction

References

1. Khosa, A.A.; Xu, T.; Xia, B.Q.; Yan, J.; Zhao, C.Y. Technological challenges and industrial applications of $CaCO_3$/CaO based thermal energy storage system—A review. *Sol. Energy* **2019**, *193*, 618–636. [CrossRef]
2. Jimoh, O.A.; Ariffin, K.S.; Hussin, H.B.; Temitope, A.E. Synthesis of precipitated calcium carbonate: A review. *Carbonat. Evaporit.* **2018**, *33*, 331–346. [CrossRef]
3. Yoo, S.; Hsieh, J.S.; Zou, P.; Kokoszka, J. Utilization of calcium carbonate particles from eggshell waste as coating pigments for ink-jet printing paper. *Bioresour. Technol.* **2009**, *100*, 6416–6421. [CrossRef] [PubMed]
4. Yan, W.; Liang, B.; Li, W.; Huang, H.; Shi, D.; Chen, Z.; Li, Z.; Yu, M.; Wei, G.; Huang, K. Study on the growth mechanism of porous spherical calcium carbonate synthesized by carbonization controlled by amino acids. *J. Solid State Chem.* **2024**, *329*, 124370. [CrossRef]
5. Yu, J.; Zhao, X.; Cheng, B.; Zhang, Q. Controlled synthesis of calcium carbonate in a mixed aqueous solution of PSMA and CTAB. *J. Solid State Chem.* **2005**, *178*, 861–867. [CrossRef]
6. Pour, G.T.; Moghadam, S.M.M. Optimization of nano calcium carbonate production process using Taguchi method. *Int. J. Mater. Mech. Manuf.* **2014**, *2*, 77–80. [CrossRef]
7. Niu, Y.-Q.; Liu, J.-H.; Aymonier, C.; Fermani, S.; Kralj, D.; Falini, G.; Zhou, C.-H. Calcium carbonate: Controlled synthesis, surface functionalization, and nanostructured materials. *Chem. Soc. Rev.* **2022**, *51*, 7883–7943. [CrossRef]
8. Babou-Kammoe, R.; Hamoudi, S.; Larachi, F.; Belkacemi, K. Synthesis of $CaCO_3$ nanoparticles by controlled precipitation of saturated carbonate and calcium nitrate aqueous solutions. *Can. J. Chem. Eng.* **2012**, *90*, 26–33. [CrossRef]
9. El-Sheikh, S.M.; El-Sherbiny, S.; Barhoum, A.; Deng, Y. Effects of cationic surfactant during the precipitation of calcium carbonate nano-particles on their size, morphology, and other characteristics. *Colloids Surf. A Physicochem. Eng. Asp.* **2013**, *422*, 44–49. [CrossRef]
10. Dagaonkar, M.V.; Mehra, A.; Jain, R.; Heeres, H.J. Synthesis of $CaCO_3$ nanoparticles by carbonation of lime solutions in reverse micellar systems. *Chem. Eng. Res. Des.* **2004**, *82*, 1438–1443. [CrossRef]
11. Kang, S.H.; Hirasawa, I.; Kim, W.-S.; Choi, C.K. Morphological control of calcium carbonate crystallized in reverse micelle system with anionic surfactants SDS and AOT. *J. Colloid Interface Sci.* **2005**, *288*, 496–502. [CrossRef] [PubMed]
12. Qian, K.; Shi, T.; Tang, T.; Zhang, S.; Liu, X.; Cao, Y. Preparation and characterization of nano-sized calcium carbonate as controlled release pesticide carrier for validamycin against Rhizoctonia solani. *Microchim. Acta* **2011**, *173*, 51–57. [CrossRef]
13. Sugih, A.K.; Shukla, D.; Heeres, H.J.; Mehra, A. $CaCO_3$ nanoparticle synthesis by carbonation of lime solution in microemulsion systems. *Nanotechnology* **2007**, *18*, 035607. [CrossRef] [PubMed]
14. Tai, C.Y.; Chen, C.-k. Particle morphology, habit, and size control of $CaCO_3$ using reverse microemulsion technique. *Chem. Eng. Sci.* **2008**, *63*, 3632–3642. [CrossRef]
15. Huber, M.; Stark, W.J.; Loher, S.; Maciejewski, M.; Krumeich, F.; Baiker, A. Flame synthesis of calcium carbonate nanoparticles. *Chem. Commun.* **2005**, 648–650. [CrossRef]
16. Tsuzuki, T.; Pethick, K.; McCormick, P.G. Synthesis of $CaCO_3$ nanoparticles by mechanochemical processing. *J. Nanoparticle Res.* **2000**, *2*, 375–380. [CrossRef]
17. Sargheini, J.; Ataie, A.; Salili, S.M.; Hoseinion, A.A. One-step facile synthesis of $CaCO_3$ nanoparticles via mechano-chemical route. *Powder Technol.* **2012**, *219*, 72–77. [CrossRef]
18. Baláž, P.; Achimovičová, M.; Baláž, M.; Billik, P.; Cherkezova-Zheleva, Z.; Criado, J.M.; Delogu, F.; Dutková, E.; Gaffet, E.; Gotor, F.J.; et al. Hallmarks of mechanochemistry: From nanoparticles to technology. *Chem. Soc. Rev.* **2013**, *42*, 7571–7637. [CrossRef]
19. Takacs, L. Self-propagating reactions induced by mechanical alloying. *Material Matter.* **2007**, *2.4*, 21.
20. Petrović, S.; Rožić, L.; Jović, V.; Stojadinović, S.; Grbić, B.; Radić, N.; Lamovec, J.; Vasilić, R. Optimization of a nanoparticle ball milling process parameters using the response surface method. *Adv. Powder Technol.* **2018**, *29*, 2129–2139. [CrossRef]
21. Zhou, F.; Ouyang, L.; Zeng, M.; Liu, J.; Wang, H.; Shao, H.; Zhu, M. Growth mechanism of black phosphorus synthesized by different ball milling techniques. *J. Alloys Compd.* **2019**, *784*, 339–346. [CrossRef]

22. Takacs, L.; McHenry, J.S. Temperature of the milling balls in shaker and planetary mills. *J. Mater. Sci.* **2006**, *41*, 5246–5249. [CrossRef]
23. Patil, A.G.; Anandhan, S. Influence of planetary ball milling parameters on the mechano-chemical activation of fly ash. *Powder Technol.* **2015**, *281*, 151–158. [CrossRef]
24. Suryanarayana, C. Mechanical alloying and milling. *Prog. Mater. Sci.* **2001**, *46*, 1–184. [CrossRef]
25. Deepika; Hait, S.K.; Chen, Y. Optimization of milling parameters on the synthesis of stearic acid coated $CaCO_3$ nanoparticles. *J. Coat. Technol. Res.* **2014**, *11*, 273–282. [CrossRef]
26. Catauro, M.; Tranquillo, E.; Dal Poggetto, G.; Pasquali, M.; Dell'Era, A.; Vecchio Ciprioti, S. Influence of the heat treatment on the particles size and on the crystalline phase of TiO_2 synthesized by the sol-gel method. *Materials* **2018**, *11*, 2364. [CrossRef]
27. Gopi, S.P.; Subramanian, V.K.; Palanisamy, K. Synergistic effect of EDTA and HEDP on the crystal growth, polymorphism, and morphology of $CaCO_3$. *Ind. Eng. Chem. Res.* **2015**, *54*, 3618–3625. [CrossRef]
28. Chao, W.; Chunde, P.; Daqing, W.; Aixia, S.; Jihong, N.; Shuhua, L. An improved method for quantitative analysis of sedimentary minerals by X-ray diffraction. *Powder Diffr.* **1996**, *11*, 235–239. [CrossRef]
29. Devarajan, A.; Khadar, M.A.; Chattopadhyay, K. Effect of ball milling on chemically synthesized nanoparticles of $CaCO_3$. *Mater. Sci. Eng. A* **2007**, *452–453*, 395–400. [CrossRef]
30. Wang, W.; Wang, S.; Liu, Q.; Wang, X.; Zhu, J.; Luo, H.; Ji, S. Study on the efficacy of amorphous calcium carbonate as a consolidant for calcareous matrix. *Herit. Sci.* **2022**, *10*, 165. [CrossRef]
31. Siva, T.; Muralidharan, S.; Sathiyanarayanan, S.; Manikandan, E.; Jayachandran, M. Enhanced polymer induced precipitation of polymorphous in calcium carbonate: Calcite aragonite vaterite phases. *J. Inorg. Organomet. Polym. Mater.* **2017**, *27*, 770–778. [CrossRef]
32. Radha, A.V.; Forbes, T.Z.; Killian, C.E.; Gilbert, P.U.P.A.; Navrotsky, A. Transformation and crystallization energetics of synthetic and biogenic amorphous calcium carbonate. *Proc. Natl. Acad. Sci. USA* **2010**, *107*, 16438–16443. [CrossRef] [PubMed]
33. Tsuzuki, T. Mechanochemical synthesis of metal oxide nanoparticles. *Commun. Chem.* **2021**, *4*, 143. [CrossRef] [PubMed]
34. Li, Y.X.; Chen, W.F.; Zhou, X.Z.; Gu, Z.Y.; Chen, C.M. Synthesis of CeO_2 nanoparticles by mechanochemical processing and the inhibiting action of NaCl on particle agglomeration. *Mater. Lett.* **2005**, *59*, 48–52. [CrossRef]